Diagrammatics for finite-temperature reaction rates

Naoki Ashida
Department of Physics, Osaka City University, Sumiyoshi-ku, Osaka 558, Japan

Hisao Nakkagawa* and Akira Niégawa†
Centre de Physique Théorique, Ecole Polytechnique, 91128 Palaiseau CEDEX, France

Hiroshi Yokota‡
Institute for Natural Science, Nara University, 1500 Misasagi-cho, Nara 631, Japan
(Received 24 September 1991)

We give a diagrammatic algorithm for calculating the reaction rate of a generic process taking place in a thermal reservoir in equilibrium. The derivation is performed by introducing a specific path in the complex-time plane and employing the path-integral method, and thus the algorithm is formulated within the framework of a real-time thermal field theory.

PACS number(s): 11.10.Ef, 05.90.+m, 12.38.Mh

I. INTRODUCTION AND SUMMARY

With the rapid progress in heavy-ion collision experiments [1], the formation of the quark-gluon plasma (QGP) in laboratory systems has come to be real, and the generic dynamical process taking place in the QGP together with the properties of the QGP itself come to be actual important physical subjects to be investigated in great detail. In this sense it is urgent to develop an efficient method to calculate the reaction rate of any given dynamical process taking place in a heat bath.

Up until now, a general prescription to calculate the thermal reaction rate for a generic process in the heat bath has not been available. The only exception is the rule to evaluate the thermal single-particle decay (production) rate, which can be expressed in terms of the thermal two-point functions. For more general processes, e.g., even the two-particle scattering process, we have had no general prescriptions to evaluate their reaction rates.

Recently the rules (the diagrammatic algorithm) that work for any thermal reactions have been formulated [2]. The derivation is, however, rather heuristic in the sense that it is based on the idea of statistical mechanics and the average over a statistical ensemble is directly taken. This algorithm, regarded as a generalization of the Cutkosky rules at zero temperature ($T=0$), is formulated in terms of the circled diagrams [3,4] with corresponding diagrammatic rules. With this algorithm it is shown [2] that the imaginary part of a forward "scattering" amplitude of physical fields in real-time thermal field theory (RTFT) is expressed as a *sum* of reaction rates of various reactions taking place in the heat bath, and thus has no direct physical relevance.

The purpose of this paper is to present a more elegant derivation of the same diagrammatic algorithm as in Ref. [2]. The present approach consists of introducing a specific path in the complex-time plane (as shown in Fig. 1 below) and employing the path-integral method. One of the new outcomes from the present approach is that the circled-diagram rules formulated in Ref. [4] are nothing but the Feynman rules in the RTFT formulated on the choice of the above real-time path [5] (see also [6–10]). This RTFT is introduced in Ref. [5], which we refer simply to as CD-RTFT (circled-diagrammatic RTFT) hereafter. It is worth mentioning that the beautiful circling rules of Kobes and Semenoff [3,4] to make up a set of circled diagrams are introduced to evaluate the imaginary part of a given causal amplitude, and thus cannot be used for evaluating the reaction rate for a generic thermal process, except for thermal one-particle decay and production.

We show that any circled diagram representing some specific reaction rate can be cut into two diagram segments: one represents the S-matrix element part and the other the S^*-matrix element part (a generalized Cutkosky

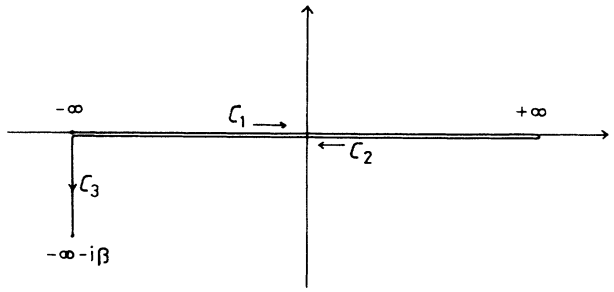

FIG. 1. The time path $C=C_1+C_2+C_3$ on the complex-time plane. The segments C_1+C_2 are the so-called "closed-time path".

*On leave of absence from Institute for Natural Science, Nara University, 1500 Misasagi-cho, Nara 631, Japan.

†Now at Department of Physics, Osaka City University, Osaka, Japan. (Electronic address: a51769@jpnkudpc.bitnet.

‡Electronic address: hyokota@jpnrifp.bitnet.

rule). This fact enables us to get a visible image of how the physical process is going.

Also discussed are rules on how to calculate the imaginary parts of physical Green's functions other than the time-ordered one (which is fully analyzed in Refs. [3–4]), such as the retarded and advanced Green's functions that are directly relevant to physical quantities.

II. INELASTIC "LEPTON" SCATTERING OFF OF CONSTITUENTS IN A "QUARK-GLUON" PLASMA

For definiteness, we examine the inelastic scalar-lepton scattering off of neutral scalars ϕ's in a heat bath of thermal ϕ's. The techniques and results, however, are general enough and thus can be applied to any reaction.

Let us now consider a grand-canonical ensemble consisting of a huge number of identical systems. The interaction Lagrangian of the system is

$$\mathcal{L}_{\rm int}=e\psi^*\psi A+\frac{e}{2}\phi^2 A+\frac{\lambda}{3!}\phi^3+\mathcal{L}_{\rm counter}\ , \tag{1}$$

where ψ, A, and ϕ stand for the complex-scalar "lepton," massless neutral scalar "photon," and neutral scalar ϕ constituting a heat bath, respectively. We are to adopt a renormalization condition

$$\mathrm{Tr}e^{-\beta H}\phi(x)/\mathrm{Tr}e^{-\beta H}=\mathrm{Tr}e^{-\beta H}A(x)/\mathrm{Tr}e^{-\beta H}=0\ .$$

Therefore, strictly speaking, it is necessary to include terms linear in ϕ and in A in $\mathcal{L}_{\rm int}$. Although we simply decline to write down these terms explicitly in Eq. (1), inclusion of them does not obstruct our following derivation, so that our conclusion is not spoiled. The following arguments do not depend on the explicit form of $\mathcal{L}_{\rm int}$.

We pick up one system out of the grand-canonical ensemble and consider the inclusive process taking place in this system:

$$\psi(p)+\text{heat bath}\rightarrow\psi(p')+\text{anything}\ ,$$

where $p(p')$ stands for the momentum of the incident (scattered) lepton. In the lowest order in e, the relevant S-matrix element is

$$S(\phi',p';\phi,p)=\frac{-ie^2}{q^2+i\varepsilon}\int d^4x\, e^{-iq\cdot x}{}_{\rm out}\langle\phi'|J(x)|\phi\rangle_{\rm in}\ , \tag{2a}$$

$$J(x)=\phi^2(x)/2\ , \tag{2b}$$

where $q=p-p'$ is the momentum of the virtual photon, and $|\phi\rangle_{\rm in}$ and $|\phi\rangle_{\rm out}$ are, respectively, the initial and final state of the system considered, which are defined by $|\phi\rangle_{\rm in,out}\equiv|\phi;t=\mp\infty\rangle$. Here $|\phi;t\rangle$, with the spatial argument of ϕ suppressed, is the eigenstate vector of the Heisenberg operator $\phi_H(r,t)$ [8,11],

$$\phi_H(r,t)|\phi(r);t\rangle=\phi(r)|\phi(r);t\rangle\ , \tag{3}$$

and these state vectors form a complete set of states:

$$\int D\phi|\phi;t\rangle\langle\phi;t|=1\ . \tag{4}$$

The transition rate of the reaction is given by

$$R(\phi',p';\phi,p)=\frac{1}{(2\pi)^4\delta(0)}\frac{1}{2|\mathbf{p}|}S^*(\phi',p';\phi,p)\times S(\phi',p';\phi,p)\ , \tag{5}$$

which describes the reaction rate *per unit volume* and *per unit incident flux*. Inserting Eq. (2) into Eq. (5), and summing over the final ϕ states, we get the differential transition rate

$$D(p';\phi,p)\equiv 2p_0'\frac{dR(p';\phi,p)}{d^3p'}=\frac{e^4}{2|\mathbf{p}|(2\pi)^3}\left[\frac{1}{q^2}\right]^2\times\int d^4x\, e^{iq\cdot x}{}_{\rm in}\langle\phi|J(x)J(0)|\phi\rangle_{\rm in}\ , \tag{6}$$

where use has been made of Eq. (4) with $t=+\infty$. $D(p',p)$, the differential transition rate, is evaluated by taking the statistical average over the grand-canonical ensemble:

$$D(p',p)=\frac{\int D\phi\, e^{-\beta E(\phi)}D(p';\phi,p)}{\int D\phi' D\phi\, e^{-\beta E(\phi)}|{}_{\rm out}\langle\phi'|\phi\rangle_{\rm in}|^2}\ , \tag{7}$$

where $E(\phi)$ is the energy of the in state $|\phi\rangle_{\rm in}$.

Substituting Eq. (6) into Eq. (7), we have

$$D(p',p)=\frac{e^4}{2|\mathbf{p}|(2\pi)^3}\left[\frac{1}{q^2}\right]^2\tilde{G}(q)\ , \tag{8}$$

where

$$\tilde{G}(q)=\int d^4x\, e^{iq\cdot x}G(x,0)\ , \tag{9a}$$

$$G(x,0)=\frac{\int D\phi_{\rm in}\langle\phi|e^{-\beta H}J(x)J(0)|\phi\rangle_{\rm in}}{\int D\phi_{\rm in}\langle\phi|e^{-\beta H}|\phi\rangle_{\rm in}}\ , \tag{9b}$$

with H the total Hamiltonian. The approach adopted in Ref. [2] is to directly perform the statistical average in Eq. (9b) as well as the sum over the final states, the sum which we already did in going to Eq. (6).

Going into the interaction picture [5], Eq. (9b) takes the form

$$G(x,0)=\frac{\int D\phi\langle\phi|e^{-\beta H_0}U_\beta\tilde{T}[J(x)U^\dagger]T[J(0)U]|\phi\rangle}{\int D\phi\langle\phi|e^{-\beta H_0}U_\beta U^\dagger U|\phi\rangle}\ , \tag{10}$$

$$U=1+\sum_{n=1}^{\infty}\frac{(-i)^n}{n!}\int_{-\infty}^{+\infty}\prod_{i=1}^{n}dt_i\,T[H_{\rm int}(t_1)\cdots H_{\rm int}(t_n)]\ , \tag{11}$$

$$U_\beta = 1 + \sum_{n=1}^{\infty} \frac{(-i)^n}{n!} \int_0^\beta \prod_{i=1}^{n} d\tau_i T_\tau [H_{\rm int}(-\infty - i\tau_1) \cdots H_{\rm int}(-\infty - i\tau_n)] , \tag{12}$$

with $H_{\rm int}$ the interaction Hamiltonian. $\tilde{T}$ in Eq. (10) stands for taking the anti-T-ordered product, T_τ in Eq. (12) is the symbol of the τ-ordered product, and all quantities in Eqs. (10)–(12) are those defined in the interaction picture, e.g., $U = U(+\infty, -\infty)$ is the time-evolution operator from $t = -\infty$ to $t = +\infty$ in the interaction picture.

Now we introduce the path in the complex-time plane [5] as shown in Fig. 1. This is a time-path C with three segments C_1, C_2, and C_3, i.e., $C = C_1 + C_2 + C_3$, which goes from $-\infty$ to $+\infty$ along the real-time axis (C_1), then returns back from $+\infty$ to $-\infty$ also along the real-time axis (C_2), and finally goes down vertically to $-\infty - i\beta$ (C_3).

In Eq. (10) the time argument 0 of the current $J(0)$ and the time arguments in the time-evolution operator U, which sweep from $-\infty$ to $+\infty$ [see Eq. (11)], lie on the segment C_1, x_0 of $J(x)$ and the time arguments in $U^\dagger$ lie on the segment C_2 and those in U_β on the segment C_3. We assume the direction along the path C, to which the arrow flows in Fig. 1, to be "future" direction. Then introducing the generalized time-path ordering operator T_C along C, we can trivially write

$$U_\beta \tilde{T}[J(x)U^\dagger] T[J(0)U] = T_C[J(x)J(0)U_\beta U^\dagger U] . \tag{13}$$

Noting that $U^\dagger$ and U_β can be written as

$$U^\dagger = 1 + \sum_{n=1}^{\infty} \frac{(-i)^n}{n!} \times \int_{C_2} \prod_{i=1}^{n} dt_i T_C[H_{\rm int}(t_1) \cdots H_{\rm int}(t_n)] , \tag{14a}$$

$$U_\beta = 1 + \sum_{n=1}^{\infty} \frac{(-i)^n}{n!} \times \int_{C_3} \prod_{i=1}^{n} dt_i T_C[H_{\rm int}(t_1) \cdots H_{\rm int}(t_n)] , \tag{14b}$$

we can show that $U_\beta U^\dagger U$ can be cast into the form

$$\mathcal{U} \equiv U_\beta U^\dagger U = 1 + \sum_{n=1}^{\infty} \frac{(-i)^n}{n!} \int_C \prod_{i=1}^{n} dt_i T_C[H_{\rm int}(t_1) \cdots H_{\rm int}(t_n)] . \tag{15}$$

Substituting this expression into Eq. (10) we have [12]

$$G(x,0) = \frac{\int D\phi \langle \phi | e^{-\beta H_0} T_C[J(x)J(0)\mathcal{U}] | \phi \rangle}{\int D\phi \langle \phi | e^{-\beta H_0} \mathcal{U} | \phi \rangle} . \tag{16}$$

Starting from this expression, through the standard argument [5,7–11,13] we arrive at the two-component theory, one of the RTFT's, in which $G(x,0)$, Eq. (16), is given as

$$G(x,0) = \frac{\delta^4}{\{[i\delta j_2(x)]^2/2\}\{[i\delta j_1(0)]^2/2\}} \exp\left\{ i \int d^4z \left[\mathcal{L}_{\rm int}\left(\frac{\delta}{i\delta j_1(z)} \right) - \mathcal{L}_{\rm int}\left(\frac{\delta}{i\delta j_2(z)} \right) \right] \right\} \times \exp\left[-\frac{i}{2} \int_{-\infty}^{+\infty} d^4\xi\, d^4\zeta \sum_{r,s=1}^{2} [j_r(\xi) D_{rs}(\xi - \zeta) j_s(\zeta)] \right] \Bigg|_{\rm conn} , \tag{17}$$

where the Fourier component of the 2×2 matrix propagator D_{rs} is given by [7]

$$D_{11}(p) = \frac{1}{p^2 - m^2 + i\varepsilon} - 2\pi i n_B(|p_0|)\delta(p^2 - m^2) , \tag{18a}$$

$$D_{22}(p) = -[D_{11}(p)]^* = \frac{-1}{p^2 - m^2 - i\varepsilon} - 2\pi i n_B(|p_0|)\delta(p^2 - m^2) , \tag{18b}$$

$$D_{12}(p) = -2\pi i[\theta(-p_0) + n_B(|p_0|)]\delta(p^2 - m^2) , \tag{18c}$$

$$D_{21}(p) = D_{12}(-p) = -2\pi i[\theta(p_0) + n_B(|p_0|)]\delta(p^2 - m^2) , \tag{18d}$$

where m is the mass of ϕ, and

$$n_B(x) = \frac{1}{e^{\beta x} - 1} . \tag{19}$$

In Eq. (17), "conn" means taking the connected part. Inserting Eq. (17) into Eqs. (8) and (9), we have the perturbative expression for the differential transition rate D.

What we have achieved is to represent the rate D by a "forward" amplitude, more precisely the one-particle-irreducible "off-diagonal" scalar photon self-energy part, in the CD-RTFT constructed on the basis of the path as in Fig. 1. Now it is easy to read out the following important fact: Mathematical tools with which our calculational rules settled above are formulated have a one-to-one correspondence with the circled-diagram rules introduced by Kobes and Semenoff [4] (see also [2]). In fact, vertices of the first- (second-) component fields correspond to the uncircled (circles) vertices, and the four types of propagators (18) have just the right correspondence to the propagators between (un)circled and (un)circled vertices. It is obvious that the reaction rate D of Eq. (8) with Eq. (17) is represented exactly by the cir-

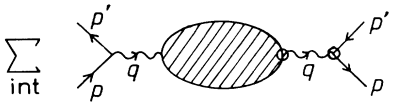

FIG. 2. The diagrammatic representation for the differential transition rate D. The solid lines denote ψ, the wavy lines ϕ, and the arrows on them express the directions to which the energies flow. The sum is taken over all possible ways of circling the internal vertices.

cled diagram depicted in Fig. 2. The sum is taken over all possible ways of circling the internal vertices.

III. DRELL-YAN PROCESS IN "QUARK-GLUON" PLASMA

In this section we study the "inverse" process to the one in the last section, namely, the scalar-"lepton" pair production in the heat bath of thermal light neutral scalar ϕ's. In quite a similar way as in the last section, we have for the differential rate P of dilepton production, heat bath $\rightarrow \psi(p)+\psi^*(p')+$anything,

$$P(p,p') \equiv 2p_0' 2p_0 \frac{dR(p,p')}{d^3p' d^3p} , \tag{20}$$

$$R(p,p') = \frac{e^4}{(2\pi)^6} \left[\frac{1}{q^2} \right]^2 \tilde{G}(-q) , \tag{21}$$

where $q = p'+p$ is the virtual-photon momentum, R is the dilepton production rate *per unit volume,* and $\tilde{G}$ is given by Eq. (9) with Eq. (16). This result is also identical with the one obtained in Ref. [2], and the graphical representation of Eq. (21) is immediately obtained as depicted in Fig. 3.

IV. PHYSICAL INTERPRETATION

To make clear the physical meaning of the results obtained in Secs. II and III, let us consider a two-loop diagram (second order in λ) contributing to the finite-temperature current-correlation function (9) with (17), as shown in Fig. 4. As mentioned in the end of Sec. II, the uncircled (circled) vertex in this figure represents the interaction vertex of the first- (second-) component field in the CD-RTFT. In fact, it can be easily seen from the analysis given in Sec. II that the uncircled vertex in Fig. 4 comes from $T[J(0)U]$ in Eq. (10), namely, from the S-matrix element part in the formula representing the inelastic lepton scattering reaction rate R, Eq. (5), while the circled vertex comes from $\tilde{T}[J(x)U^\dagger]$, namely, from the S^*-matrix element part.

These facts mean that the propagator $D_{11}(D_{22})$ between uncircled (circled) vertices represents the *thermal propagator* of the type-1 (-2) field that propagates inside the S- (S^*-) matrix element part. As is also clear from Eqs. (18a) and (18b), these propagators D_{11} and D_{22} are nothing but those of the physical and thermal ghost fields in a general RTFT [8,9], respectively. The propagator $D_{21}(p)$ $(p_0>0)$ from an uncircled vertex toward a circled one represents that of the final-state particle [involved in ${}_{\text{out}}\langle\phi|$ in Eq. (2)] "propagating" from the S part toward the S^* part [see, Eq. (5) with Eq. (2)], and $D_{12}(p)$ $(p_0>0)$ from a circled vertex toward an uncircled one represents that of the initial-state particle "propagating" from the S^* part toward the S part. Explaining with the example of Fig. 4, the propagator, say $D_{21}(p_2)$, represents for $p_{20}>0$ the propagation of the final-state particle from the S part toward the S^* part, while for $p_{20}<0$, it represents that of the initial-state particle from the S^* part toward the S part.

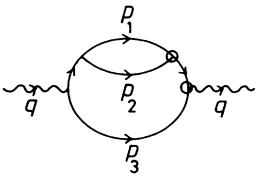

FIG. 4. Two-loop (second order in λ) circled diagram that contributes to the finite-temperature current-correlation function (9).

To clarify the above proposition, let us show here that the circled diagram shown in Fig. 4 can be expressed as a sum of "cut diagrams," any one of which has the structure $S \otimes S^*$ [Eq. (5)] and thus represents a square of the physical reaction amplitude in a heat bath. As a matter of fact, given a circled diagram, a set of cut diagrams is unambiguously determined and vice versa as codified below in the form of rules.

The cutting rules (in constructing cut diagrams). For a given circled diagram, perform a continuous deformation without changing their topological structure so that all the uncircled (circled) vertices are laid within the left (right) side of the original diagram. Cut all the propagators linking an uncircled vertex to a circled one, i.e., linking the left half to the right one. Thus, we get a "diagram" with a vertical cutting line in the middle. Then deform each piece of the cut propagator so that the positive energy flows from the left to the right direction. The left (right) portion of the diagram thus obtained represents the S- (S^*-) matrix element part in Eq. (5). This is regarded as a finite-temperature generalization of the Cutkosky or the cutting rules in vacuum theory. (Here we do not touch on the method of circling of the propagators D_{11} and D_{22}, full details of which are given in the last paper in Ref. [2]).

As an example, we take the circled diagram Fig. 4, with $q_0>0$ and $q^2<0$. Applying the above cutting rules, we can cut the diagram, Fig. 4, to get a set of cut diagrams depicted in Fig. 5. Let us pay attention to the propagator $D_{21}(p_1)$ in Fig. 4, which expresses the propagation from the uncircled vertex to the circled one. If $p_{10}>0$, then from Eq. (18d) it takes the form

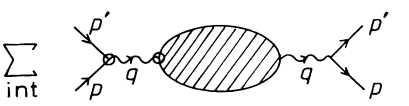

FIG. 3. The diagrammatic representation for the dilepton production rate (per unit volume) R. The meanings of the symbols are the same as in Fig. 2.

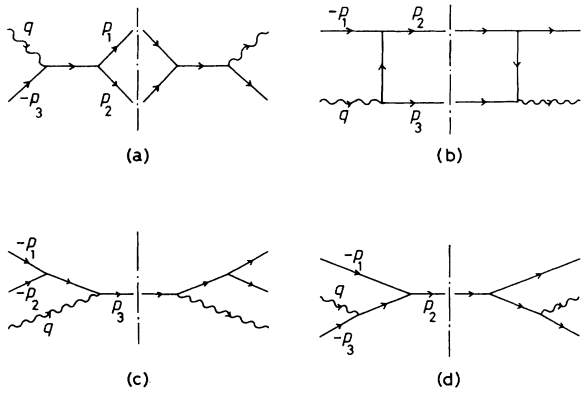

FIG. 5. Cut diagrams obtained from the circled diagram Fig. 4 with the use of cutting rules ($q_0>0$, $q^2<0$). Each diagram corresponds to the following region of the loop momenta in the circled diagram, Fig. 4: (a) p_{10} and $p_{20}>0$, $p_{30}<0$; (b) $p_{10}<0$, p_{20} and $p_{30}>0$; (c) p_{10} and $p_{20}<0$, $p_{30}>0$; (d) p_{10} and $p_{30}<0$, $p_{20}>0$.

$$D_{21}(p_1)=-2\pi i[1+n_B(p_{10})]\delta(p_1^2-m^2),\quad p_{10}>0\ , \tag{22}$$

which expresses the sum of spontaneous and stimulated emissions of ϕ quantum with momentum p_1 into the final state (i.e., the heat bath). This fact correctly reflects on the corresponding cut diagrams Fig. 5(a), which represent the region $p_{10}>0$ of the original circled diagram, Fig. 4. If $p_{10}<0$, on the other hand, $D_{21}(p_1)$ takes the form [see, Eqs. (18c) and (18d)]

$$D_{21}(p_1)=D_{12}(-p_1)=-2\pi i n_B(|p_{10}|)\delta(p_1^2-m^2)\ ,\quad p_{10}<0\ , \tag{23}$$

from which we can see that it expresses the induced absorption of the initial-state ϕ quantum (with momentum $-p_1$) from the heat bath, and that the corresponding cut diagrams, Figs. 5(b)–5(d), correctly represent this fact. Other "propagators" in Fig. 4 also have the corresponding physical interpretations in terms of the cut diagrams (namely, the physical reactions in the heat bath). Thus, we can understand that the sum of "cut diagrams" in Figs. 5 correctly represent the physical contents involved.

As another example, let us consider the circled diagram, Fig. 6, which contributes to the "Drell-Yan" process. This diagram survives only when $m=0$ with the dimensional regularization method employed to regularize the infrared divergence. Following the cutting rules stated above, we can manage to express this figure as a sum of cut diagrams as shown in Figs. 7, each of them having

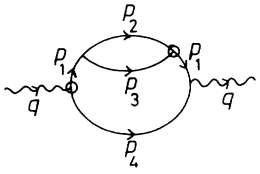

FIG. 6. Two-loop (second order in λ) circled diagram that contributes to the finite-temperature "Drell-Yan process" ($q_0>0$, $q^2>0$).

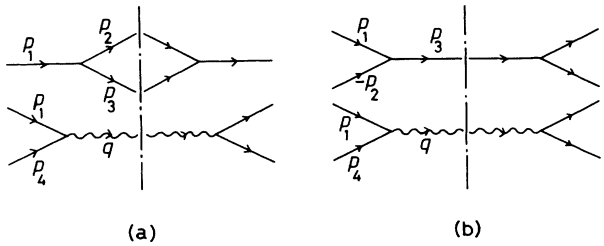

FIG. 7. Cut diagrams obtained from the circled diagram Fig. 6. Each diagram corresponds to the following region of the loop momenta in the circled diagram, Fig. 6: (a) p_{10}, p_{20}, p_{30}, and $p_{40}>0$; (b) p_{10}, p_{30}, and $p_{40}>0$, $p_{20}<0$.

the structure $S\otimes S^*$ and thus representing a squared physical reaction amplitude in a heat bath. In this example we again find for any "propagator" a right physical correspondence with the cut diagrams. For example, the propagator $D_{21}(p_2)$ in Fig. 6, which has the expression, for $p_{20}<0$,

$$D_{21}(p_2)=-2\pi i n_B(|p_{20}|)\delta(p_2^2-m^2),\quad p_{20}<0\ , \tag{24}$$

represents the induced absorption of the initial-state ϕ quantum from the heat bath. This fact is neatly expressed in the corresponding cut diagrams in Fig. 7(b).

Finally, it is worth mentioning the following: A somewhat bizarre diagram Fig. 6 has been regarded so far only as playing the "passive" role of eliminating a $[\delta(p_1^2-m^2)]^2$ singularity [4,14] and has been thought to be noncuttable. It is now obvious, however, that it really represents a set of physical processes such as those depicted in Fig. 7, and thus can be cut in the sense defined above.

V. DISCUSSION

A. Generalization

All the arguments presented so far can be straightforwardly generalized to any generic process involving more general fields. We reach the circling rules: When a thermal process is given, the rules identify a set of circled diagrams to evaluate the reaction rate. Here we give only one example. By taking the model (1), let us consider a gedanken experiment: *m virtual* scalar photons with incident momenta $k_1,k_2,\ldots,k_m$ go into a heat bath and interact with thermal ϕ's to produce *n virtual* scalar photons with outgoing momenta $k_1',k_2',\ldots,k_n'$. Then the reaction rate R of this process is represented in terms of the circled diagram depicted in Fig. 8. An analysis on the basis of cutting rules presented in Sec. IV in the cases of two-body circled diagrams that contribute to the inclusive lepton scattering and to the Drell-Yan process can also be developed in the present case straightforwardly, and leads us to a proper physical interpretation of the final formula that has a sophisticated circled-diagram expression.

B. Calculational rules for evaluating the imaginary part of Green's functions directly related to physical quantities

Here we address the following question: How can we calculate the imaginary part of Green's functions or am-

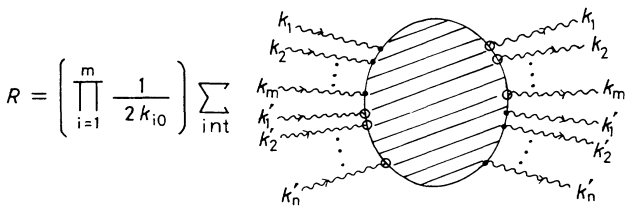

FIG. 8. The reaction rate R of a process where arbitrary numbers of scalar photons with momenta $k_1 \sim k_m$ interact and produce those with momenta $k'_1 \sim k'_n$.

plitudes other than the causal ones? What Kobes and Semenoff have established by the circled-diagram rules is the perturbative diagrammatic algorithm [3,4] in evaluating the imaginary part of a *causal* amplitude in the standard RTFT. By the standard RTFT we mean thermofield dynamics [8,15] or the RTFT based on the time path [8–11],

$$-\infty \rightarrow +\infty \rightarrow +\infty - i\beta/2 \rightarrow -\infty - i\beta/2 \rightarrow -\infty - i\beta \ ,$$

in the complex-time plane, both of which are equivalent [8–10] as far as perturbative expansions are concerned. Here let us recall the fact that the Green's functions (amplitudes) which are directly related to the physical quantities, such as the retarded and the advanced ones, can be represented [7] as linear combinations of various Green's functions (amplitudes), $\tilde{G}$'s, in the CD-RTFT which is defined on the time path depicted in Fig. 1. Also to be noted is that any such Green's function (amplitude) $\tilde{G}$ in the CD-RTFT is related to the corresponding one, G, in the standard RTFT:

$$\tilde{G} = e^{\beta\Sigma(\pm q_0)/2} G \ , \tag{25}$$

where q_0's with $+$ ($-$) sign are the outgoing (incoming) energies of the external thermal ghosts. The above Eq. (25) follows directly from the following fact [8,9]: The type-2 field $\phi_2(x)$ in the CD-RTFT and the so-called thermal-ghost (or tilde) field $\tilde{\phi}(x)$ in the standard RTFT are mutually related through the imaginary-time translation

$$\tilde{\phi}(x) = e^{\beta H/2} \phi_2(x) e^{-\beta H/2} \ . \tag{26}$$

Now the imaginary part of each G, and hence through Eq. (25), of any physical Green's function (amplitude) $\tilde{G}$, can be evaluated thanks to the algorithm settled by Kobes and Semenoff in their first paper [3].

As an example, the retarded Green's function (spatial variables suppressed)

$$G_r(t_1, t_2, \ldots, t_n) \equiv (-i)^{n-1} \sum_{(t_2, \ldots, t_n)} \theta(t_1 - t_2)\theta(t_2 - t_3) \cdots \theta(t_{n-1} - t_n) \mathrm{Tr} e^{-\beta H} [\cdots [[\phi(t_1), \phi(t_2)], \phi(t_3)], \ldots, \phi(t_n)] \tag{27}$$

with a sum being taken over all permutations of $t_2, \ldots, t_n$, is shown [7] to be represented by the linear combination

$$G_r = \sum_{x_i, z_j}^{i \neq 1} \tilde{G}(x_1, \ldots, x_n; z_j) \ , \tag{28}$$

where the sum runs over all arrangements of type-1 (uncircled) and type-2 (circled) external vertices (denoted by x's) as indicated and of type-1 and type-2 internal vertices (z's). It should be noted that the right-hand side (RHS) of Eq. (28) is equal to what Kobes writes as $\mathcal{F}_R^{(1)}$ [16] in discussing the "retarded functions" at finite temperature. Also noted is that the equality (28) has also been proved by Evans [17] for the three-point ($n = 3$) case in a somewhat different context. Using the relation of the same type as Eq. (25), we can evaluate the imaginary parts of the $i\tilde{G}$'s in Eq. (28) through the standard method presented in the first paper of Kobes and Semenoff [3], where general Green's functions including both physical and thermal-ghost fields were treated. Each term thus obtained, which constitutes $\mathrm{Im} i G_r$, may be translated back into a Green's function $\tilde{G}$ in the CD-RTFT through an analogous formula to Eq. (25). In the case of a "forward" G_r, in the light of the analysis in the present paper, we can interpret each of the final (amputated) $\tilde{G}$'s in terms of the reaction rates, i.e., the reactions taking place in a heat bath (see Sec. IV). An analysis of various Green's functions along this line will be a future work.

Finally, as an illustration of our general program, we briefly consider a simple example of two-point amputated retarded Green's function $G_r(q)$ [$\equiv -i\Sigma_r(q)$] in the $\lambda\phi^3$ theory, and study the contribution from a set of circled diagrams shown in Fig. 9. (This analysis is only for an illustrative purpose because this Σ_r has been studied already in the literature, see e.g., [16].):

$$\Sigma_r(q) = \sum_{x_2; z_1, z_2} \tilde{\Sigma}(q; x_1, x_2; z_1, z_2) \ . \tag{29}$$

With the help of Eq. (25), the RHS of Eq. (29) can be expressed in terms of Green's functions in the standard RTFT as

$$\Sigma_r(q) = \sum_{z_1, z_2} [\Sigma(q; x_1, x_2; z_1, z_2) + e^{\beta q_0/2} \Sigma(q; x_1, \underline{x_2}; z_1, z_2)] \ . \tag{30}$$

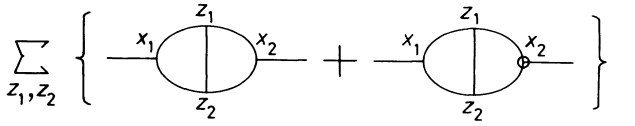

FIG. 9. Set of two-loop circled diagrams that contributes to the two-point amputated retarded Green's function $-i\Sigma_r$ in the scalar $\lambda\phi^3$ theory. The sum over z_1 and z_2 runs over all possible arrangements of type-1 and type-2 vertices.

From here to Eq. (32) below x_i ($\underline{x_i}$) denotes the vertex of the physical (thermal-ghost) field. The sum over internal vertices z_1 and z_2 runs over all possible combinations of the physical and the thermal-ghost (or tilde) vertices.

The imaginary part of each two-point Green's function (in the standard RTFT) can be evaluated through the method in Ref. [3]: e.g.,

$$\mathrm{Im}\Sigma(q;x_1,\underline{x_2};z_1,\underline{z_2}) = -\frac{i}{2}[\,\Sigma(q;x_1,\underline{x_2};z_1,\underline{z_2}) + \Sigma(q;\underline{x_1},x_2;\underline{z_1},z_2)\,] \,. \quad (31)$$

Thus, as the imaginary part of $\Sigma_r(q)$, Eq. (30), we get

$$\mathrm{Im}\Sigma_r(q) = -\frac{i}{2}(e^{\beta q_0/2} - e^{-\beta q_0/2}) \times \sum_{z_1,z_2} \Sigma(q;x_1,\underline{x_2};z_1,z_2) \,. \quad (32)$$

Now we again use Eq. (25) to rewrite the RHS of (32) in terms of corresponding Green's functions in the CD-RTFT, and finally get

$$\mathrm{Im}\Sigma_r(q) = -\frac{i}{2}\sum_{z_1,z_2}[\,\tilde{\Sigma}(q;x_1,\hat{x_2};z_1,z_2) - \tilde{\Sigma}(q;\hat{x_1},x_2;z_1,z_2)\,] \,, \quad (33)$$

where $\hat{x_i}$ denotes the vertex at the point x_i to be type 2, i.e., a circled vertex, and here again the sum over internal vertices z_i runs over all possible ways of circlings.

The physical contents of the quantities on the RHS of Eq. (33) can be disclosed through the rules developed in this paper. In fact, we can see that the first (second) $\tilde{\Sigma}$ on the RHS of Eq. (33) represents the decay (production) rate Γ_d (Γ_p) of ϕ in the heat bath, so that the quantity in Eq. (33) is proportional to the net decay rate $\Gamma_d - \Gamma_p$. This result is of course, already known [16], but we repeated it here just for the illustrative purpose of our general program.

ACKNOWLEDGMENTS

Two of us (H.N. and A.N.) would like to thank Dr. B. Pire for his hospitality extended to them. They also thank Professor R. Baier for helpful discussions and his hospitality at the Fakultät für Physik, Universität Bielefeld, FRG, where part of this work has been carried out.

[1] For a review on quark-gluon plasma, see J. Cleymans, R. V. Gavai, and E. Suhonen, Phys. Rep. **130**, 17 (1986); see also *Quark Matter '88,* Proceedings of the Seventh International Conference on Ultrarelativistic Nucleus-Nucleus Collisions, Lenox, Massachusetts, 1988, edited by G. Baym, P. Braun-Munzinger, and S. Nagamiya [Nucl. Phys. **A498**, 1 (1989)]; M. Jacob, in *Proceedings of the 25th International Conference on High Energy Physics,* Singapore, 1990, edited by K. K. Phua and Y. Yamaguchi (World Scientific, Singapore, 1991).

[2] A. Niégawa, Phys. Lett. B **247**, 351 (1990); in *Proceedings of the 2nd Workshop on Thermal Field Theories and Their Applications,* edited by H. Ezawa, T. Arimitsu, and Y. Hashimoto (Elsevier, Amsterdam, 1991); N. Ashida, H. Nakkagawa, A. Niégawa, and H. Yokota, Ann. Phys. (N.Y.) (to be published).

[3] R. L. Kobes and G. W. Semenoff, Nucl. Phys. **B260**, 714 (1985).

[4] R. L. Kobes and G. W. Semenoff, Nucl. Phys. **B272**, 329 (1986).

[5] R. Mills, *Propagators for Many-Particle Systems* (Gordon and Breach, New York, 1969).

[6] J. Schwinger, J. Math. Phys. **2**, 407 (1961); L. V. Keldysh, Zh. Eksp. Teor. Fiz. **47**, 1515 (1964) [Sov. Phys. JETP **20**, 1018 (1965)]; R. A. Craig, J. Math. Phys. **9**, 605 (1968).

[7] K.-C. Chou, Z.-B. Su, B.-L. Hao, and L. Yu, Phys. Rep. **118**, 1 (1985).

[8] N. P. Landsman and Ch. G. van Weert, Phys. Rep. **145**, 141 (1987).

[9] H. Matsumoto, Y. Nakano, and H. Umezawa, J. Math. Phys. **25**, 3076 (1984).

[10] H. Matsumoto, Y. Nakano, H. Umezawa, F. Mancini, and M. Marinaro, Prog. Theor. Phys. **70**, 599 (1983).

[11] A. J. Niemi and G. W. Semenoff, Ann. Phys. (N.Y.) **152**, 105 (1984); Nucl. Phys. **B230** [FS10], 181 (1984).

[12] A similar expression has once been considered by Niemi in a different context: A. J. Niemi, Phys. Lett. B **203**, 425 (1988).

[13] A. Niégawa, Phys. Rev. D **40**, 1199 (1989).

[14] R. Baier, B. Pire, and D. Schiff, Phys. Rev. D **38**, 2814 (1988); W. Keil, *ibid.* **40**, 1176 (1989); T. Altherr, P. Aurenche, and T. Becherrawy, Nucl. Phys. **B315**, 436 (1989).

[15] Y. Takahashi and H. Umezawa, Collect. Phenom. **2**, 55 (1975); H. Umezawa, H. Matsumoto, and M. Tachiki, *Thermo Field Dynamics and Condensed States* (North-Holland, Amsterdam, 1982).

[16] R. Kobes, Phys. Rev. D **43**, 1269 (1991).

[17] T. S. Evans, Phys. Lett. B **249**, 286 (1990); **252**, 108 (1990).